Appropriately regularized OSEM can improve the reconstructed PET images of data with low count statistics

Konstantinos Karaoglanis[1,2] MSc,
Irene Polycarpou[1,3] PhD,
Nikos Efthimiou[4,5] PhD,
Charalampos Tsoumpas[1,5,6] PhD

1. Dept. of Biomedical Engineering, Division of Imaging Sciences and Biomedical Engineering, Kings College London, United Kingdom
2. Dept. of Biomedical Technology, Biomedical Research Foundation of the Academy of Athens, Greece
3. School of Sciences, Nicosia, European University of Cyprus
4. Dept. of Biomedical Engineering, Technological Educational Institute of Athens, Greece
5. Division of Biomedical Imaging, University of Leeds, United Kingdom
6. Translational and Molecular Imaging Institute and Dept. of Radiology, Icahn School of Medicine at Mount Sinai, New York, USA

Keywords: PET simulated data,
- Low statistic counts,
- Regularized OSEM,
- Less noise,
- Reduced injected dose

Correspondence address:
Charalampos Tsoumpas, PhD,
8.001a, Worsley Building,
Clarendon Way, University
of Leeds, Leeds, LS2 9JT,
West Yorkshire, United Kingdom
C.Tsoumpas@leeds.ac.uk

Received:
5 May 2015
Accepted:
20 June 2015

Abstract

Objective: With the increasing number of patients undergoing positron emission tomography (PET) scans and the fact that multiple whole body acquisitions are performed during therapy monitoring, the reduction of scan time as well as of the injected radioactive dose are important issues. However, short scan time and reduction of the injected radiation dose result in low count statistics, which significantly affects the quality of the reconstructed images and accurate diagnosis. The aim of this study was to explore the effect of low count statistics on ordered subset expectation maximization regularized with median root prior (OS-MRP-OSL) reconstructed images. **Methods**: By optimizing OS-MRP-OSL we determined whether a satisfactory handling of the noise properties and bias can be achieved compared to post-filtered ordered subset expectation maximization (OSEM), which will lead to improved image quality in simulations with more noise. We used realistic simulated PET data of a thorax with lesions corresponding to tumors with different intensities. **Results**: OS-MRP-OSL provided reduced noise from post-filtered OSEM, without having the negative effect of blurring. On the other hand, bias presented no significant difference. **Conclusion**: This work is relevant to future PET reconstruction of clinical images and PET-magnetic resonance investigations where the reduced injected dose will allow imaging a larger cohort of humans.

Hell J Nucl Med 2015; 18(2): 140-145 *Epub ahead of print: 19 July 2015* *Published online: 5 August 2015*

Introduction

Positron emission tomography (PET) images give physiological and metabolic information based on the distribution of radiotracers inside the body of the patient. Quantitative and semi-quantitative information can be obtained to help the diagnosis and characterize various abnormalities such as cancerous lesions [1-4]. Positron emission tomography images are highly affected with noise and the use of iterative image reconstruction can provide images with reasonable image quality. Nevertheless, several iterations are required to obtain accurate value particularly for small regions with relatively low uptake. However, the iteratively reconstructed images are substantially affected by noise after a large number of iterations and image quality is severely degraded. In order to optimise both quantitative accuracy and image quality regularized iterative reconstruction algorithms have been proposed in the literature. These algorithms offer better results than only filtering the images reconstructed with existing commercial algorithms. Regularized iterative reconstruction methods are now implemented incommercial systems (e.g. Q. Clear™ software marketed by GE Healthcare). The images obtained with regularized reconstruction algorithms will potentially help the nuclear medicine physicians to diagnose with higher accuracy plausible pathological conditions.

Further than this, the increasing number of patients undergoing PET scans and the fact that multiple whole body acquisitions are performed during therapy monitoring, the reduction of scan time as well as of the injected radioactive dose are important issues. Short scan times can increase the patient throughput giving the opportunity to busy centres to scan more patients every day and the possibility of performing interscans to follow-up treatment. Furthermore, shorter in time acquisitions are less affected by motion artefacts and may even boost the use of radiotracers with shorter half-life. The reduction of the injected dose can be translated to reduced patient and staff exposure to radioactivity. Moreover, it will be greatly beneficial for cases where low amount of injected dose is crucial. However, short scan time and reduction of injected radiation dose result in low count statistics [5, 6].

Consequently, the reconstructed images present even higher increased bias and are prone to high noise that could affect the tumour detectability and accuracy of classification [7-10]. Previous studies demonstrated the benefits in image quality by using smoothing filters or advanced reconstruction algorithms including regularization [11-13].

Other researchers [14, 15] have used two algorithms; the first was a negative maximum likelihood algorithm (NEG-ML) [16] and the second was an OSEM using upper and lower bounds for the image values (AB)-OSEM, which removes the non-negativity constraint in the reconstructed images, in order to deal with the increasing bias which is observed in OSEM [17]. They showed that AB-OSEM outperforms NEG-ML and can remove the bias on the expense of increased standard deviation. In another study [16], a different version of the NEG-ML algorithm including corrections of the sources of contamination with the ordinary Poisson OSEM scheme (OP-NEG3D), was evaluated. It was thus shown that OP-OSEM had better noise and bias characteristics than filtered back-projection (FBP) and OP-OSEM [16].

On the other hand, it was shown that scanner resolution model (RM)-OP-OSEM reduces the variance of values in the voxels and bias is reduced but not eliminated [18]. Comparison between regularized versus non-regularized statistical reconstruction techniques concluded that non-regularized iterative reconstruction algorithms tend to be noisier in low-count regions [19]. Algorithms like maximum likelihood-expectation maximization (MLEM) and OSEM give the opportunity for a better modelling but at the same time noise propagation is observed over iterations. By using a priori probabilities, accuracy may be improved while maintaining image quality [20]. Various filter types have been proposed and evaluated. Other researchers used Metz filters to obtain better contrast against OSEM and post-filtered OSEM [21].

Further validation on phantom and clinical studies showed that the Ordered Subsets Median Root Prior One Step Late (OS-MRP-OSL) algorithm could reach a stable solution with preservation of spatial details and noise reduction for both high and low statistics [22]. The noise reduction against FBP and post-filtered FBP has been discussed previously [20]. The importance of optimal parameterization in MRP-OSL for regularization on motion correction algorithms has also been presented previously [23].

The aim of this study was to explore the effect of low statistics on OS-MRP-OSL reconstructed images using a widely used open source software library. The selection of the regularization parameter is crucial to the image quality and to quantitative accuracy but no robust is available in a practical automatic way to set this parameter, which among others depends on the number of measured coincidences. By optimizing OS-MRP-OSL parameters we determined whether a satisfactory handling of the noise properties and bias can be achieved compared to post filtered OSEM. Contrast to noise ratio (CNR), root mean squared error (RMSE), bias, standard deviation (STD) and coefficient of variation (CoV) were used as figures of merit to investigate the accuracy and quality of the reconstructed images. We used realistic PET data of a thorax phantom, analytically simulated from MR data with introduced lesions corresponding to tumours with different accumulated activities and sizes.

Materials and Methods

Simulation procedure

Magnetic resonance (MR) data from a 1.5T Philips Achieva™ scanner, using an ultra-short time-echo (UTE) sequence were obtained. The 3D MR images were segmented and used to produce realistic emission and attenuation data for a Philips Gemini PET scanner. This methodology has been previously described in detail [24, 25] and the data are available to the research community under the licence described at http://www.isd.kcl.ac.uk/pet-mri/simulated-data/.

In brief, the emission data were created, by assigning typical standard uptake values (SUV) in the segmented MR images. Alike, the attenuation images were created by assigning the corresponding attenuation values [26]. The emission and attenuation values that were used are displayed in Table 1.

For the purpose of this study five different datasets were produced introducing different amounts of Poisson noise in the emission data. As a reference we used, Poisson noise corresponding to a typical 5min 3D fluorine-18-fluorodexyglucose (^{18}F-FDG) scan with 65×10^6 counts [24, 25] including scatter coincidences. The simulated datasets corresponded to scans with lower statistics than the reference ones and are presented in Table 2.

Table 1. *Attenuation and emission values, for different types of tissue, used in the phantom*

Region	Attenuation values (cm^{-1})	Emission values
Air	0	0
Lung	0.03	0.5
Soft tissue	0.099	1
Bone	0.15	2.3
Liver	0.099	2.5
Myocardium	0.099	3.2

Table 2. *Counts corresponding to different Poisson noise levels, for each dataset*

Dataset ID:	1	2	3	4	5
Counts ($x10^6$)	4.68	9.37	14.1	23.4	42.2

Introduction of lesions

Nine spherical lesions corresponding to tumours were analytically inserted in the phantom in the same manner as described previously [23]. All lesion characteristics are presented in Table 3. The different backgrounds were used as a substitute to ensemble noise due to the absence of multiple noise realizations of the simulated dataset [28].

Reconstruction

The OS-MRP-OSL algorithm was originally presented by Green (1990 and 1990) [30, 31] and later was implemented in software for tomographic image reconstruction (STIR) [32], an open source library reconstruction of PET and single photon emission tomography (SPET) images [33], (http://stir.sf.net). Equation 1 demonstrates the OS-MRP-OSL [20]:

$$\lambda_{OSL}^{new} = \frac{1}{1+\beta\frac{\lambda(i)-Med(\lambda,i)}{Med(\lambda,i)}\,|\,\lambda=\lambda_{OSL}^{old}}\lambda_{OSEM}^{new}$$

Where λ is the image, i is the pixel, β is the weight of the median root prior (MRP), Med (λ,i) is the median of a block, known also as kernel, of neighbour pixels (e.g. 3×3×3, 5×5×5). The size of the median kernel of OS-MRP-OSL was 3×3×3 voxels to ensure that the smallest possible details would be preserved. Bettinardi et al. (2002) [22] have shown that details with half the size of the median kernel filter are preserved. A range of β was employed in order to explore the effect of small (1, 5), medium (10, 50) and large (75, 100) values. By deploying the aforementioned values, the trade-offs for different count levels are to be observed. The penalization factors were constant throughout the reconstructions.

In the case of post-filtered OSEM, different Gaussian filters (i.e. 3×3×3mm^3, 4×4×4mm^3, 5×5×5mm^3, 6×6×6mm^3 and 12×12×12mm^3) were applied to the result of each iteration.

Table 3. *Lesions characteristics*

Lesions number	Diameter (mm)	SUV	Surrounding tissue
1	14	9.5	Liver
2	14	7.5	Diaphragm
3	14	7.5	Lung
4	14	6.5	Liver
5	14	4.5	Diaphragm
6	14	4.5	Lung
7	8	6.5	Liver
8	8	4.5	Diaphragm
9	8	4.5	Lung

Wilcoxon signed rank test

In order, to assess whether the values have stabilized after a number of iterations we have used the Wilcoxon signed rank statistical significance test. The aforementioned test was chosen because the measurements may not follow a normal distribution. We defined the statistical significance threshold to 0.009. The values of bias, RMSE and CoV, which is defined as the ratio of the STD over the mean were compared after every iteration for all lesions. A u-value less than 0.009 indicated that there was a statistical significance.

Figures of merit

The results were assessed by comparing the following figures of merit. The values were calculated taking into account edge voxels. For the particular investigation we selected lesions 2, 6 and 7. Lesions 2 and 6 had the largest diameter (14mm) but different SUV values and resided in regions with different background level. On the other hand, lesion 7 had the smallest diameter of 8mm, SUV value in between the other two and resided in a tissue with high background contribution.

CNR calculation

The CNR was calculated according to the formula:

$$CNR = \frac{m_{Li} - m_{Bi}}{m_{Bi} \times \sigma_{Bi}}$$

Where, m_{Li} is the mean value of the radioactivity distribution in the i^{th} lesion and m_{Bi} and σ_{Bi} are the mean and STD values of the corresponding background region of interest (ROI). The background ROI for each lesion was of the same size and resided in the same type of tissue.

The σ_{Bi} was calculated using the formula:

$$\sigma = \sqrt{\frac{\sum x^2}{N} - \mu^2}$$

Where, x is the value of each voxel in the ROI, N is the number of voxels and μ the mean value of the ROI.

Regional RMSE calculation

We used RMSE to evaluate the results in terms of accuracy and precision, as it expresses the agreement between the estimated and the real image in a normalized quantitative measure.

Root MSE was defined by the following equation:

$$RMSE_j = \sqrt{Bias_j^2 + \sigma_j^2}$$

Where bias over a region j was defined as:

$$bias_j = mean_{orig\,j} - mean_j$$

Where *mean j* is the mean of a region j in the reconstructed images and $mean_{origj}$ is the mean of the same region in the noiseless original image.

Results

Wilcoxon signed rank test

The Wilcoxon signed rank test showed that when large β was deployed, no significant change in terms of bias, RMSE and CoV, was presented after 10 iterations. For β=50, p values were 0.066, 0.066, 0.173 for bias, RMSE and CoV respectively, while for β=100 the corresponding values were 0.767, 0.26 and 0.173.

For low β values and for standard OSEM there seemed to be a significant change (u<0.009), for the aforementioned quantitative values even after 10 iterations. Based on the results of the test we decided that 10 iterations was a reasonable point to stop and evaluate the results.

Visual comparison

The coronal views of the region of thorax (lesions 3, 6 and 9), for three different noise levels (datasets "1", "2" and "3") reconstructed with OS-MRP-OSL with different β values and OSEM post-filtered with different Gaussian filters, are presented in Figure 1.

The results demonstrated that reduced Poisson noise ensures an improved visual quality, as expected. For β=0 (Figures 1a, 1b and 1c), the images are extremely noisy, affecting the lesion detectability. One must note that OS-MRP-OSL for β=0 is the conventional OSEM.

The use of higher β values (second and third lines) strongly improved the image quality for all datasets. While the image quality on the least noisy dataset "5" has been improved the beneficial impact on datasets "1" and "4" is higher.

In the case of post-filtered results (4th and 5th lines of Figure 1), the images are also improved compared to conventional OSEM. The smoothing effect of the Gaussian filters reduced the impact of the noise, but, on the same time introduced strong blur in the images.

Visual comparison provided clear indications for the superior performance of OS-MRP-OSL over post-filtered OSEM, in terms of contrast and image blurring.

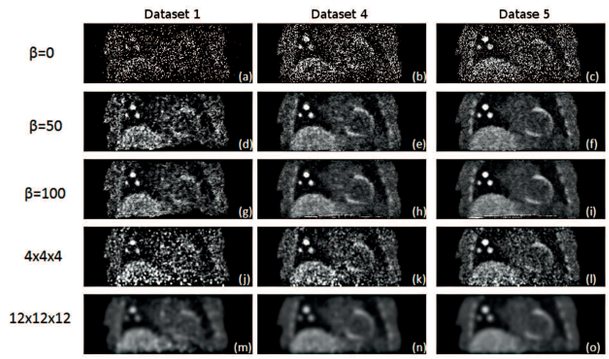

Figure 1. Coronal views of the thorax region with lesions 3, 6 and 9 for different noise levels, reconstructed with OS-MRP-OSL (top three rows) and post-filtered OSEM (bottom two rows), are presented.

CNR and RMSE

CNR and RMSE over β for lesions 2, 6 and 7 after 10 iterations, are displayed in Figure 2. For lesions 2 and 7, convergence and maximum CNR are achieved for β=50. Lesion 6 displayed the tendency to improve further with β in all datasets, except, dataset "5" which has already successfully converged. For β=50, CNR was almost doubled.

Root MSE, in most cases presented the lowest value for β=10 or β=50. At the most noisy dataset, improvement of up to 50% was presented.

In Table 4 the CNR and RMSE values of post-filtered OSEM for dataset "2", are presented. In all cases the 4mm filter exhibited better performance than 12mm, both in terms of CNR as well as RMSE.

Comparing the values provided by OS-MRP-OSL to post-filtered OSEM, one could see that after proper selection of β, CNR and RMSE were strongly improved.

Bias over STD

Bias versus standard deviation for OS-MRP-OSL for lesions 2, 6 and 7, and β ranging from 1 to 100, are presented in Figure 2 (left column).

The graphs show that increased β leads to reduced STD

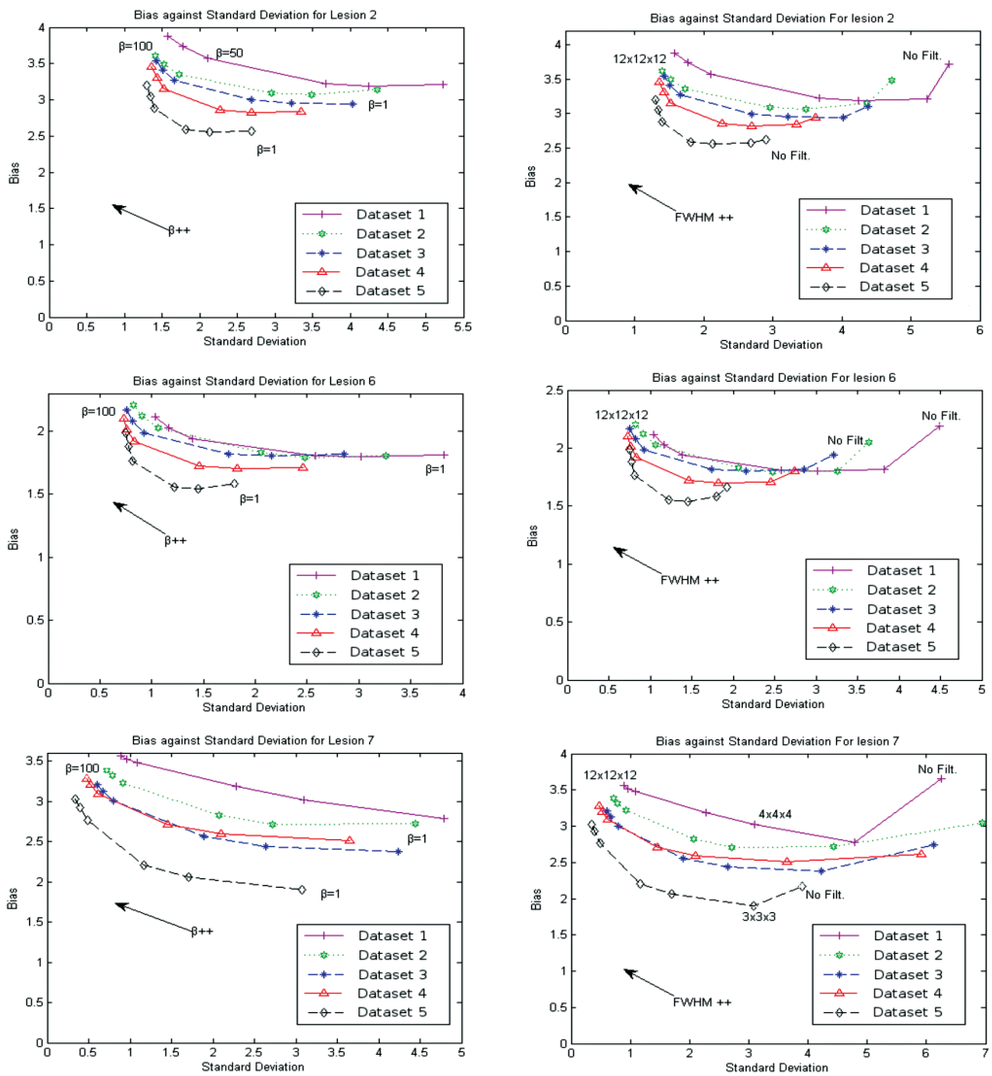

Figure 2. Bias over STD for lesions 2, 6 and 7 reconstructed with OS-MRP-OSL with various β (left column) and post-filtered OSEM with different Gauss filters (right column) are presented.

***Table 4**. CNR and RMSE values for dataset "2": OSEM images filtered with a range of Gaussian filters of different FWHM: 4mm and 12mm*

Lesion ID:	2		6		7	
FWHM	4mm	12mm	4mm	12mm	4mm	12mm
CNR:	23.80	19.90	10.60	9.10	0.56	0.54
RMSE:	3.68	3.61	2.32	2.3	3.05	3.05

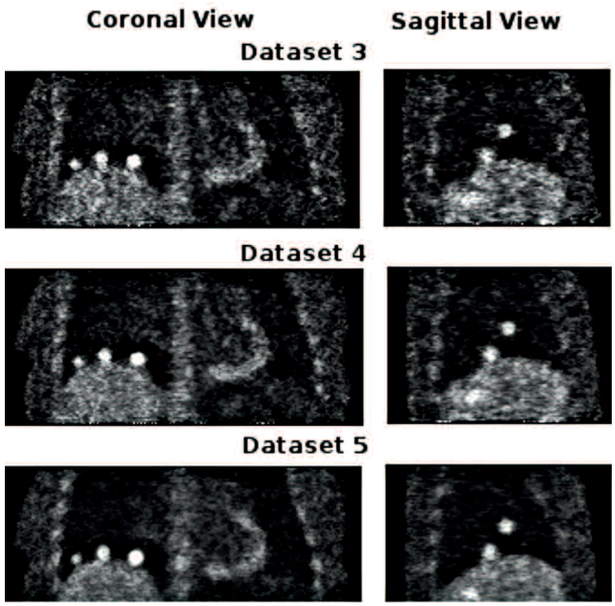

Figure 3. Coronal and sagittal views of reconstructed images using OS-MRP-OSL with β=50 after 10 iterations with 23 subsets. Results for datasets "3", "4" and "5", are displayed.

for all datasets, especially those with high introduced noise levels. In the nosiest dataset "1", the presented STD improvement was more than 70% while when β was >75 a rise on the bias, of approximately 7%, was observed in all cases.

Alike, bias over STD for post-filtered OSEM images of different Gaussian filters, are presented in Figure 2 (right column). The results for dataset "1" showed improvement of the STD approximately 75%-80% accompanied by a 17% rise on bias.

Discussion

Visual comparison in Figures 1 and 4 demonstrated that OS-MRP-OSL could limit the impact of the noise level of the data without introducing the negative effects of blurring as post-filtered OSEM. In lesions 2 and 7 OS-MRP-OSL, with β>50, provided higher CNR, than post-filtered OSEM in most cases. The amount of introduced noise in the datasets affected the convergence of the algorithm.

In terms of RMSE both algorithms performed in a similar manner. The results displayed a strong dependence on the amount of introduced noise in the dataset and the contribution of the background area.

Investigation on bias and STD showed that, if was β>50, OS-MRP-OSL provided significantly lower STD and similar bias, compared to post-filtered OSEM. One can see that for FWHM 12mm, the values of post-filtered OSEM were similar to OS-MRP-OSL, but in the expense of resolution degradation as illustrated in Figure 1.

Taking into account all the aforementioned results, Figure 3 presents the coronal and sagittal views of the images reconstructed from the three lowest noise levels, using β=50. In the coronal view, the lesions placed on the diaphragm are pictured (lesions 2, 3, 8). In the sagittal view, lesions 7, 5 and 6, are visible.

The evaluation of other priors (e.g. quadratic, anatomical priors) and reconstruction algorithms (e.g. AB-OSEM, NEG-ML) may unveil new prospects. It will also be very interesting to investigate the reaction of OS-MRP-OSL with the Cramer-Rao bound [34] and include TF and PSF information in the reconstruction.

This work is relevant to PET-MR investigation where the need for reduced injected dose is more relevant than in PET/CT studies as they are not limited by the CT dose [35]. Furthermore, regularized reconstruction and optimization of the penalization parameter according to the injected dose, tracer, patient size and age will become issues of research in the clinical context when these algorithms will be used routinely (e.g. the recent reconstruction software marketed by GE: Q. Clear™) [36-37]. The familiarity with the reconstructed images by the physicians is another factor that will require more time and effort for these algorithms to be used in the clinic. However, once they become available it will be helpful in identifying and staging tumors and other small pathological conditions more accurately.

In conclusion, visual, as well as, quantitative comparison between OS-MRP-OSL and post-filtered OSEM provided indications that under proper configuration, both can improve the diagnostic value of noisy data. The iterative reconstruction algorithm OS-MRP-OSL can surpass post-filtered OSEM in terms of CNR and STD, avoiding the negative impact of blurring in the images. In terms of bias and RSME both algorithms demonstrated similar performance.

Acknowledgements
Mr K. Karaoglanis would like to thank the research staff of the Biomedical Research Foundation of the Academy of Athens (A. Gaitanis and G. Spyrou) for the suggestions and fruitful discussions and the IT staff at King's College London (A. Cantell and D. Poccecai) for their excellent continuous support in using the HPC. This project was completed with multiple travel support from the EU COST Action (TD1007, http://www.pet-mri.eu) for K. Karaoglanis, N. Efthimiou and C. Tsoumpas.

The authors declare that they have no conflicts of interest.

Bibliography

1. Karpetas GE, Michail CM, Fountos G.P. Towards the optimization of nuclear medicine procedures for better spatial resolution, sensitivity, scan image quality and quantitation measurements by using a new Monte Carlo model featuring PET imaging. *Hell J Nucl Med* 2010; 13(2): 166-8.
2. Promteangtrong C, Salavati A, Cheng G et al. The role of positron emission tomography-computed tomography/magnetic resonance imaging in the management of sarcoidosis patients. *Hell J Nucl Med* 2014; 17(2): 123-35.
3. Kong EJ, Chun KA,Bom HS et al. Initial experience of integrated PET/MR mammography in patients with invasive ductal carcinoma. *Hell J Nucl Med* 2014; 17(3):171-6.
4. Artiko V, Odalovic S, Sobic-Saranovic D et al. Can ^{18}F-FDG PET/CT scan change treatment planning and be prognostic in recurrent col orectal carcinoma? A prospective and follow-up study. *Hell J Nucl Med* 2015; 18(1): 35-41.
5. Verdun FR. Patient dose and image quality: role of medical physicists. *Phys Medica* 2014; 30: e1.
6. Poon JK, Dahlbom ML, Moses WW et al. Optimal whole-body PET scanner configurations for different volumes of LSO scintillator: a simulation study. *Phys Med Biol* 2012; 57: 4077-94.
7. Polycarpou I, Tsoumpas C, Marsden PK. Analysis and comparison of two methods for motion correction in PET imaging. *Med Phys* 2012; 39(10): 6474-83.
8. Efthimiou N, Loudos G, Karakatsanis NA, Panayiotakis GS. Effect of ^{176}Lu intrinsic radioactivity on dual head PET system imaging and data acquisition, simulation and experimental measurements. *Med Phys* 2013; 40(11): 112505.
9. Schäfers KP. The promise of nuclear medicine technology: Status and future perspective of high-resolution whole-body PET. *Phys Medica* 2008; 24: 57-62.
10. Freedenberg MI, Badawi RD, Tarantal AF, Cherry SR. Performance and limitations of positron emission tomography (PET) scanners for im aging very low activity sources. *Phys Medica* 2014; 30: 104-10.
11. Bourhis D, Andrieux A, Abgrall R, Salaün PY et. al. Ultra low-dose CT feasibility with statistical iterative reconstruction for anatomical localization in PET-CT imaging. *Phys Medica* 2011; 27: S18.
12. Xie L, Hu Y, Wang Z, Luo L. Projection space MAP method for low photon count PET image reconstruction. *Shuju Caiji Yu Chuli/Journal of Data Acquisition and Processing* 2011; 26: 41-6.
13. Kim K, Son YD, Bresler Y et al. Dynamic PET reconstruction using temporal patch-based low rank penalty for ROI-based brain kinetic analysis. *Phys Med Biol* 2015; 60: 2019-46.
14. Verhaeghe J, Reader AJ. AB-OSEM reconstruction for improved Patlak kinetic parameter estimation: a simulation study. *Phys Med Biol* 2010;21; 55(22): 6739-57.
15. Letourneau E, Verhaeghe J, Reader AJ. Impact of tracer distribution, count level, iterations and post-smoothing on PET quantification using a variously weighted least squares algorithm. 2012 *IEEE Nucl Sci Symp Med Imag Conf Rec*, 2351-3.
16. Grezes-Besset L, Nuyts J, Boellard R et al. Simulation-based evaluation of NEG-ML iterative reconstruction of low count PET data. 2007 *IEEE Nucl Sci Symp Med Imag Conf Rec*, 3009-14.
17. Erlandsson K, Visvikis D, Waddington W et. al. Low-statistics reconstruction with AB-EMML. 2000 *IEEE Nucl Sci Symp Med Imag Conf Rec*, 249-53.
18. Walker MD, Asselin MC, Julyan PJ et. al . Bias in iterative reconstruction of low-statistics PET data: benefits of a resolution model. *Phys Med Biol* 2011; 56(4): 931-49.
19. Denisova NV. Regularized versus non-regularized statistical reconstruction techniques. *Nucl Instr Meth Phys Res A* 2011; 648, Supplement 1:S65-7.
20. Alenius S, Ruotsalainen U. Bayesian image reconstruction for emission tomography based on median root prior. *Eur J Nucl Med Mol Imaging* 1997; 24(3): 258-65.
21. Jacobson M, Levkovitz R, Ben-Tal A et al. Enhanced 3D PET OSEM reconstruction using inter-update Metz filtering. *Phys Med Biol* 2000; 45(8): 2417-39.
22. Bettinardi V, Pagani E, Gilardi M et. al. Implementation and evaluation of a 3D one-step late reconstruction algorithm for 3D positron emission tomography brain studies using median root prior. *Eur J Nucl Med*. 2002; 29(1): 7-18.
23. Tsoumpas C, Polycarpou I, Thielemans K et. al. The effect of regularization in motion compensated PET image reconstruction: a realistic numerical 4D simulation study. *Phys Med Biol* 2013; 58(6): 1759-73.
24. Tsoumpas C, Buerger C, King AP et. al. Fast generation of 4D PET-MR data from real dynamic MR acquisitions. *Phys Med Biol* 2011; 56(20): 6597-613.
25. Tsoumpas C, Gaitanis A. Modeling and Simulation of 4D PET-CT and PET-MR Images. *PET Clin*. 2013; 8(1): 95-110.
26. Buerger C, Tsoumpas C, Aitken A et al. Investigation of MR-based attenuation correction and motion compensation for hybrid PET/MR. *IEEE Trans Nucl Sci* 2012; 59(5): 1967-76.
27. Surti S, Kuhn A, Werner ME et al. Performance of Philips Gemini TF PET/CT scanner with special consideration for its Time-of-Flight imaging capabilities. *J Nucl Med* 2007; 48: 471-80.
28. Tong S, Alessio AM, Kinahan PE. Noise and signal properties in PSF-based fully 3D PET image reconstruction: an experimental evaluation. *Phys Med Biol* 2010; 55(5): 1453-73.
29. Alenius S, Ruotsalainen U, Astola J. Using local median as the location of the prior distribution in iterative emission tomography image reconstruction. IEEE *Trans Nucl Sci* 1998; 45(6): 1726-30.
30. Green PJ. Bayesian reconstructions from emission tomography data using a modified EM algorithm. IEEE *Trans Med Imag* 1990; 9(1): 84-93.
31. Green PJ. On use of the EM algorithm for penalized likelihood estimation. *J R Stat Soc* 1990; 52: 443-52.
32. Thielemans K, Tsoumpas C, Mustafovic S et. al. STIR: software for to mographic image reconstruction release 2. *Phys Med Biol* 2012; 57(4): 867-83.
33. Fuster BM, Falcon C, Tsoumpas C et al. Integration of advanced 3D SPECT modelling into the open-source STIR framework. Med Phys 2013; 40(9): 092502.
34. Cloquet C, Defrise M. MLEM and OSEM Deviate from the Cramer-Rao bound at low counts. IEEE Trans Nucl Sci 2013; 60(1): 134-43.
35. Eldib M, Bini J, Lairez O et. al. Feasibility of ^{18}F-Fluorodeoxyglucose radiotracer dose reduction in simultaneous carotid PET/MR imaging. *Am J Nucl Med Mol Imaging* 2015; 5(4): 401-7.
36. Grecchi E, Thielemans K, Cook GJ, Tsoumpas C. Influence of three reconstruction algorithms on the estimation of the standardize uptake value in ^{18}F-fluoride PET. *IEEE Nucl Sci Symp Med Imag* 2013 *Conf Rec*, 1-5.
37. Ahn S, Ross SG, Asma E et al. Quantitative comparison of OSEM and penalized likelihood image reconstruction using relative difference penalties for clinical PET. *Phys Med Biol* 2015; 60: 5733-51.